J. metamorphic Geol., 2006, **24,** 3–18 doi:10.1111/j.1525-1314.2005.00618.x

Deformation-enhanced metamorphic reactions and the rheology of high-pressure shear zones, Western Gneiss Region, Norway

M. P. TERRY AND F. HEIDELBACH
Bayerisches Geoinstitut, Universität Bayreuth, 95440 Bayreuth, Germany (michael.terry@uni-bayreuth.de)

ABSTRACT Microstructural and petrological analysis of samples with increasing strain in high-pressure (HP) shear zones from the Haram garnet corona gabbro give insights into the deformation mechanisms of minerals, rheological properties of the shear zone and the role of deformation in enhancing metamorphic reactions. Scanning electron microscopy with electron backscattering diffraction (SEM–EBSD), compositional mapping and petrographic analysis were used to evaluate the nature of deformation in both reactants and products associated with eclogitization. Plagioclase with a shape-preferred orientation that occurs in the interior part of layers in the mylonitic sample deformed by intracrystalline glide on the (0 0 1)[1 0 0] slip system. In omphacite, crystallographic preferred orientations indicate slip on (1 0 0)[0 0 1] and (1 1 0)[0 0 1] during deformation. Fine-grained garnet deformed by diffusion creep and grain-boundary sliding. Ilmenite deformed by dislocation glide on the basal and, at higher strains, prism planes in the **a** direction. Relationships among the minerals present and petrological analysis indicate that deformation and metamorphism in the shear zones began at 500–650 °C and 0.5–1.4 GPa and continued during prograde metamorphism to ultra-high-pressure (UHP) conditions. Both products and reactants show evidence of syn- and post-kinematic growth indicating that prograde reactions continued after strain was partitioned away. The restriction of post-kinematic growth to narrow regions at the interface of garnet and plagioclase and preservation of earlier syn-kinematic microstructures in older parts layers that were involved in reactions during deformation show that diffusion distances were significantly shortened when strain was partitioned away, demonstrating that deformation played an important role in enhancing metamorphic reactions. Two important consequences of deformation observed in these shear zones are: (i) the homogenization of chemical composition gradients occurred by mixing and grain-boundary migration and (ii) composition changes in zoned metamorphic garnet by lengthening diffusion distances. The application of experimental flow laws to the main phases present in nearly monomineralic layers yield upper limits for stresses of 100–150 MPa and lower limits for strain rates of 10^{-12} to 10^{-13} s^{-1} as deformation conditions for the shear zones in the Haram gabbro that were produced during subduction of the Baltica craton and resulted in the production of HP and UHP metamorphic rocks.

Key words: eclogite; garnet; high-pressure metamorphism; ilmenite; Norway; omphacite; plagioclase; rheology; shear zone; strain rate; subduction; Western Gneiss Region.

INTRODUCTION

In high-pressure (HP) and ultra-high-pressure (UHP) terranes, where relatively dry rocks (e.g. granitoids, gabbro and orthogneiss) are carried to great depths during continental subduction, the growth of new metamorphic minerals is commonly localized in shear zones. This observation led to the conclusion that deformation plays an important role in enhancing metamorphic reactions with more favourable kinetics or faster diffusion (Koons *et al.*, 1987). More recent studies have highlighted the important role of fracturing and fluid infiltration in catalysing metamorphic reactions which allows a more complete transformation to an eclogite assemblage (e.g. Boundy *et al.*, 1992; Früh-Green, 1994; Austrheim *et al.*, 1998; Glodny *et al.*, 2003; John & Schenk, 2003). Direct evidence includes pseudotachylite formation, veins and fractures with eclogite assemblages at their margins, as well as growth of hydrous phases such as zoisite and phengite. In a general model for eclogitization of relatively dry continenal crust, these observations comprise the early phase (Austrheim *et al.*, 1998). The later parts of this model involves the localization of ductile strain in the areas around fractures or veins or fractures where transformation to an eclogite assemblage was taking place. The formation of the HP phases is proposed to be connected with a weakening of the rock (referred to as transformation plasticity) which may result from the formation of new weaker phases or a change in deformation mechanism (Rubie, 1983 and references therein). In this study, we examine well-described shear zones (Terry & Heidelbach, 2004; Terry & Robinson, 2004) where the direct evidence for

pseudotachylite formation, fracturing and fluid infiltration is lacking, and the rock exposure provides a clear picture of the role of ductile deformation in enhancing metamorphic reactions.

From a geodynamic perspective, shear zones have the potential to accommodate large displacements which juxtapose rocks of differing metamorphic grade and bring them to a new set of metamorphic conditions. This includes the subduction (descent) and exhumation (ascent) phases that take place during the orogenic cycle. The recognition that HP and UHP rocks have vertical velocities on the order of millimetres to centimetres per year in modern and ancient orogens may place constraints on the rheological properties of HP shear zones and the mechanisms that might be used to explain the ascent of metamorphic rocks to the surface. Thus, the rheological properties of these shear zones can have a dramatic influence on the processes that may be responsible for producing and exhuming HP and UHP metamorphic rocks during continental subduction. In this study, we examine microstructures from HP shear zones that show evidence for syn- to post-kinematic eclogitization on the prograde path (Terry & Heidelbach, 2004) which allows the effects of deformation to be assessed as a result of strain being partitioned away or removed from the shear zone while prograde metamorphism was ongoing. In addition, the microstructural observations allow insights into the rheological properties of HP shear zones which include linking microstructural and experimental observations to give insights into strain rate and stress under eclogite facies conditions and the memory of crystallographic preferred orientations (CPOs) associated with partial recrystallization.

GEOLOGICAL AND TECTONIC SETTING

The study area is located in the Western Gneiss Region (Fig. 1a), which is an erosional window through overlying thrust nappes and allochthons that were transported and stacked on the former craton of Baltica during the Scandian Orogeny (425–375 Ma). This window has the best exposures of HP and UHP rocks in the world. On Nordøyane (Fig. 1b), strain partitioning has resulted in the preservation of eclogite-facies structural features which are described by Terry & Robinson (2003, 2004) and Terry & Heidelbach (2004). The Haram gabbro (Fig. 1c) is a classic coronitic gabbro (1466 ± 2 Ma) with shear zones that were formed by top-SE shearing during subduction of Baltica beneath Laurentia. The gabbro crosscuts dioritic gneiss (Ulla gneiss) (1654 ± 2 Ma) in the northern unit which is composed of the Ulla Gneiss, metamorphosed gabbro, and granitic gneiss and may have an age of 410 ± 1 Ma based on detailed structural analysis and U-Pb zircon dating in the nearby Flem Gabbro (Fig. 1b) (Ravna & Terry, 2004). Outside shear zones, the gabbro shows development of garnet coronas around pre-existing mafic minerals controlled by diffusion of elements and the reactions are dependent on the bulk composition of the gabbro (Mørk, 1985; Cox & Indares, 1999). The two major types of coronas include the following minerals from core to rim: (i) omphacite + garnet + plagioclase or igneous pyroxene + omphacite + garnet + plagioclase and (ii) ilmenite ± rutile + garnet + plagioclase. In quartz-bearing grabbroic rocks and the coronas are interpreted by to have grown by the general reaction:

$$\begin{aligned}&\text{orthopyroxene/clinopyroxene} + \text{plagioclase}\\ &= \text{garnet} + \text{omphacite} + \text{Na plagioclase}\\ &\quad + \text{kyanite} + \text{quartz}.\end{aligned} \tag{1}$$

In some of the gabbro compositions, quartz is absent except as rare inclusions in omphacite. Textural relations among the minerals present indicate that the development of type 1 coronas and gneissic layers in gabbro mylonite were produced by the general reactions:

$$\begin{aligned}&\text{Ca plagioclase} + \text{orthopyroxene/clinopyroxene}\\ &\quad + \text{spinel} = \text{omphacite} + \text{garnet}\\ &\qquad + \text{Na-plagioclase} + \text{kyanite}\end{aligned} \tag{2}$$

and type 2 coronas by the general reaction:

$$\begin{aligned}&\text{Ca plagioclase} + \text{ilmenite} + \text{spinel}\\ &= \text{rutile} + \text{garnet} + \text{Na plagioclase} + \text{kyanite}.\end{aligned} \tag{3}$$

SAMPLES

Oriented samples were cored in the Haram Gabbro (Fig. 1) ranging from undeformed gabbro far from a shear zone to highly deformed ultramylonite inside a shear zone (Fig. 2). Sections were cut normal to the foliation and parallel to the lineation in the shear zone. With increasing strain the gabbro was progressively changed from a typical igneous textured garnet corona gabbro (Fig. 2a) to a mylonitic micro-gneiss (Fig. 2c) similar to that described by Williams *et al.* (2000), and finally to an ultramylonite (Fig. 2e), where the layering becomes extremely thin resulting in a more homogeneous appearance. Samples also show an increasing degree of foliation and lineation with decreasing distance to the shear zone. The foliation is mainly formed by layers of plagioclase, omphacite, garnet and mixed ilmenite–magnetite bands. Their thickness decreases with increasing deformation. The lineation is due to extended corona structures around the mafic minerals.

ANALYTICAL METHODS

Thin sections were prepared from each sample and used for electron microprobe mapping and quantitative analysis. The same face from which the thin section was removed was polished by standard methods (SiC and diamond to 0.5 μm). For the scanning electron microscopy with electron backscattering

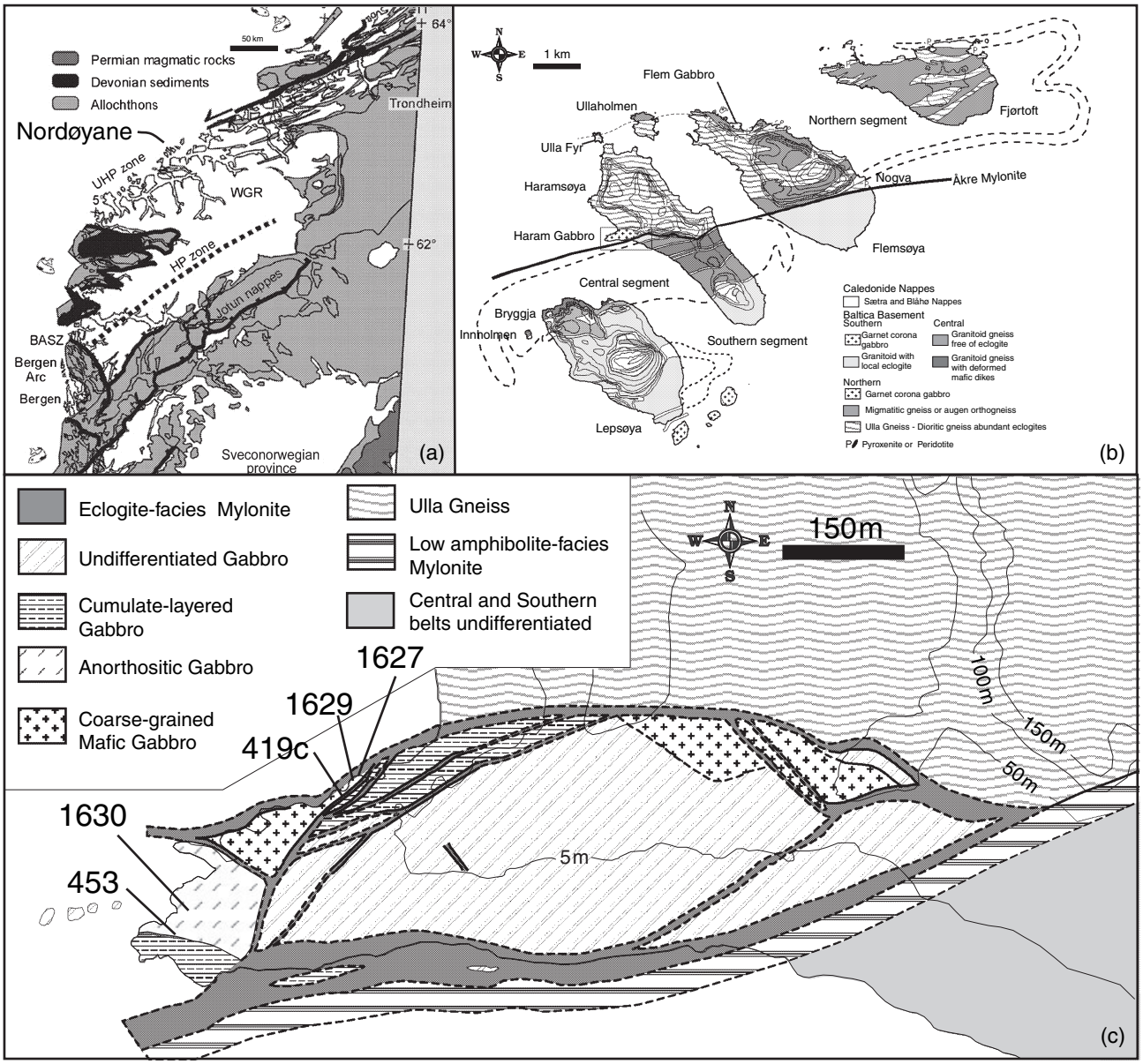

Fig. 1. (a) Geological map of the Western Gneiss Region located in southwest Norway. (b) Geological map of Nordøyane from Terry & Robinson (2004). Box shows the location of the Haram Gabbro. (c) Geological map of the Haram gabbro showing the sample locations.

diffraction (SEM-EBSD) analysis, an additional step of combined etching and polishing was performed with a high-pH colloidal silica solution (40 nm particle size) in order to remove the surface layer damaged by previous polishing. The samples were then coated with *c*. 4 nm of carbon to reduce charging and possible beam drift during the orientation measurements.

Mineral compositions were determined using a Cameca SX-50 microprobe at Bayerisches Geoinstitut with an accelerating voltage of 15 keV, a beam current of 15 nA and counting times of 20 s. Matrix corrections were performed using the PAP method (Pouchou & Pichoir, 1984a,b). Images showing compositions of different elements were made both on the Cameca SX-50 and a Jeol 8500 electron microprobe at Bayerisches Geoinstitut applying beam currents of *c*. 100, *c*. 500 and *c*. 750 nA and rastering the stage with a fixed electron beam.

The analysis of microstructures and lattice preferred orientations (CPOs) was carried out with a SEM (LEO Gemini 1530 with a Schottky emitter) using the EBSD technique (Adams *et al*., 1993). SEM-EBSD allows determination of the complete orientation of the crystal underneath the beam with micron resolution.

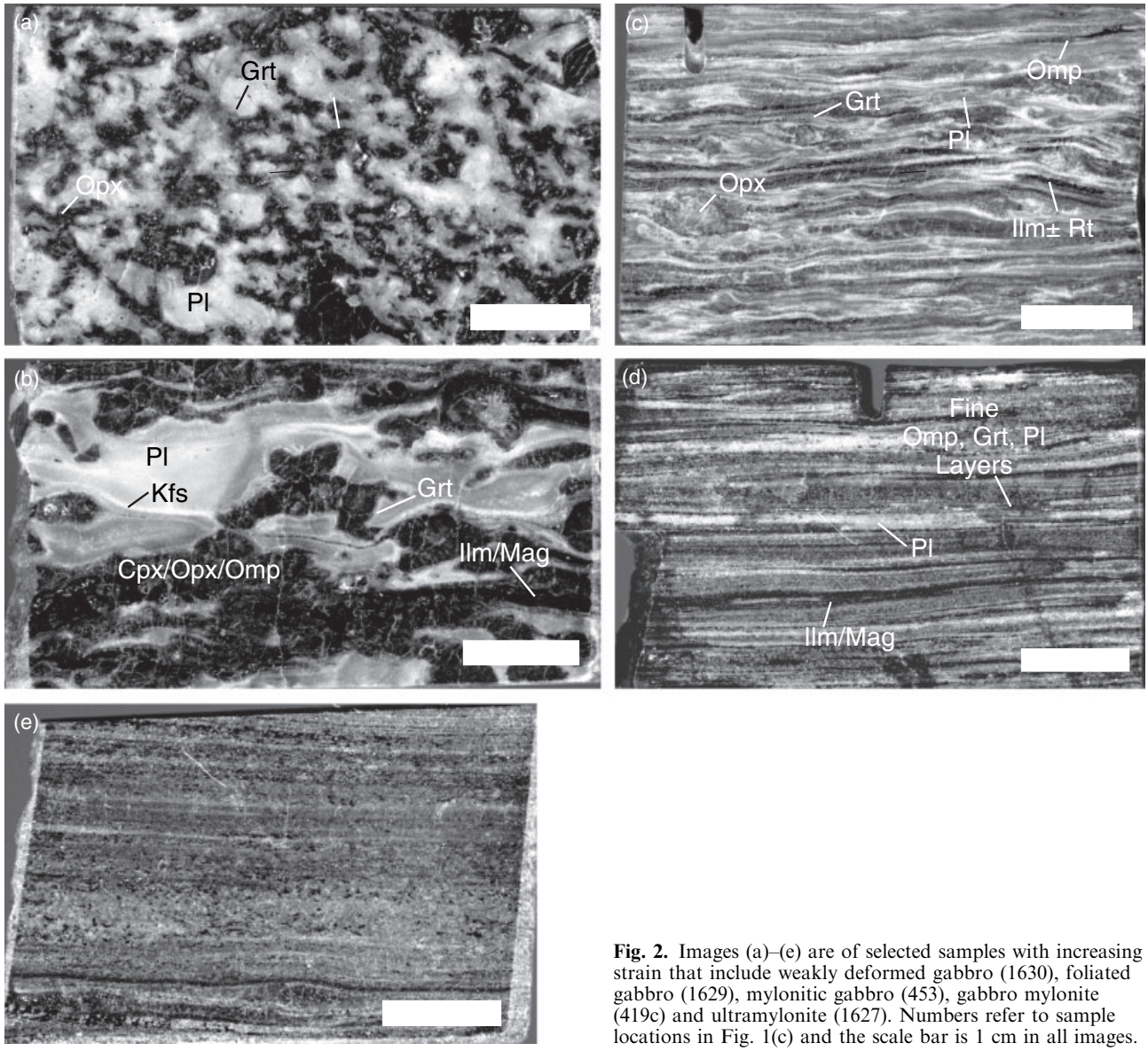

Fig. 2. Images (a)–(e) are of selected samples with increasing strain that include weakly deformed gabbro (1630), foliated gabbro (1629), mylonitic gabbro (453), gabbro mylonite (419c) and ultramylonite (1627). Numbers refer to sample locations in Fig. 1(c) and the scale bar is 1 cm in all images.

The CPO of a bulk sample can be mapped out by analysing automatically the crystal orientations from a large number of points on the sample surface. In this study, we took scans of various sizes (from a few square millimetre up to thin section scale) for the different phases; as the overall CPO for each phase was of main interest, step sizes were also rather large (up to 200 μm) such that each grain was measured only a few times. The beam current was about 3.5 nA and the accelerating voltage was set to 20 keV. In each scan, only one phase was analysed in order to avoid complications of misindexing between different phases. In order to avoid false indexing the minimum number of reflections used for the calculation of the correct orientation, the solution was set to six (theoretically only three non-cozonal reflections are sufficient) and the mean angular deviation of these six reflections was not allowed to be greater than 1.5°. Although misindexings occurred in some cases (e.g. a garnet was indexed as omphacite or vice versa), comparison between SEM-EBSD measurements and backscattered images showed that these were rare exceptions and had practically no influence on the bulk CPO.

Scanning electron microscopy with electron backscattering diffraction data yield the complete orientation of the crystal lattice at each measuring point and a full orientation distribution function (ODF) can be directly calculated from them; however, for the sake of simplicity, data are presented here only in the form of pole figures of the most meaningful crystallographic forms for each phase. Additional microstructural information was gained from imaging the samples with

a forescatter detector which records preferentially the backscattered electrons caused by orientation differences (Prior *et al.*, 1996).

PHASE RELATIONSHIPS, MICROSTRUCTURES AND CRYSTAL PREFERRED ORIENTATION

In this section, the fabrics of the minerals that were the products and reactants of corona-forming reactions are described. Diffusion-controlled growth and interface-controlled nucleation of metamorphic minerals resulted in the growth of monomineralic layers or layers that are dominated by a single phase in foliated and mylonitic samples. This feature allows characterization of the microstructures, deformation mechanisms and relative strengths of individual minerals, and additional information on the reaction history and metamorphic evolution.

Igneous pyroxene

Relict orthopyroxene and clinopyroxene grains of magmatic origin form large porphyroclasts of up to 4 mm size with relatively little internal deformation (Figs 2c & 3a). The foliation bends around porphyroclasts and in the lineation direction they show tails of omphacite, garnet and plagioclase giving an indication of the shear sense. The porphyroclasts of orthopyroxene in foliated to mylonite samples have annealed fractures defined by clear Al-poor orthopyroxene surrounded by cloudy Al-rich orthopyroxene that contains very fine exsolution of clinopyroxene (Fig. 3; Table 1). These fractures are truncated by the omphacite that grew during metamorphism (Fig. 3b). The CPO of the relict pyroxene was not measured as their number per thin-section area was much too small (*c*. 2–3) to give conclusive results about an overall alignment of crystallographic axes.

Table 1. Selected microprobe analyses.

Mineral	Opx	Opx	Mineral	Spl
Sample	453	453	Sample	453
SiO_2	53.65	52.63	SiO_2	0.06
Al_2O_3	1.76	3.03	Al_2O_3	59.92
TiO_2	0.10	0.14	TiO_2	0.01
Cr_2O_3	0.22	0.10	Cr_2O_3	n.d.
MgO	25.37	24.84	MgO	11.47
FeO*	16.53	16.86	FeO*	27.49
MnO	0.21	0.22	MnO	0.07
CaO	2.21	1.90	CaO	0.14
Na_2O	0.09	0.20		
K_2O	0.01	0.02		
Total	100.15	99.95	Total	99.15
Si	1.950	1.920	Si	0.002
Al total	0.075	0.130	Al total	1.909
Ti	0.003	0.004	Ti	0.000
Cr^{3+}	0.006	0.003	Cr^{3+}	0.000
Mg	1.374	1.350	Fe^{3+}	0.088
Fe^{2+}	0.502	0.514	Fe^{2+}	0.534
Mn	0.006	0.007	Mg	0.462
Ca	0.086	0.074	Mn	0.002
Na	0.007	0.014	Ca	0.004
K	0.001	0.001		
Total	4.010	4.018	Total	3.000
FM	0.268	0.276	FM	0.536

Notes: n.d. Not detected.

Plagioclase layers

Plagioclase in the foliated sample occurs in large recrystallized lenses which appear to represent the feldspar grains from the original gabbro. The lenses are aligned in the foliation, but may show internally an oblique grain shape foliation (Fig. 4a). Increasing deformation causes the plagioclase lenses to form extended layers in the foliation in the mylonitic and mylonite samples. Lenses and layers are composed of fine-grain plagioclase (~50 μm), with minor amounts of kyanite and spinel (Fig. 4b). Plagioclase grains that have a preferred grain shape orientation in the mylonitic sample have Ca-rich rims that grew during

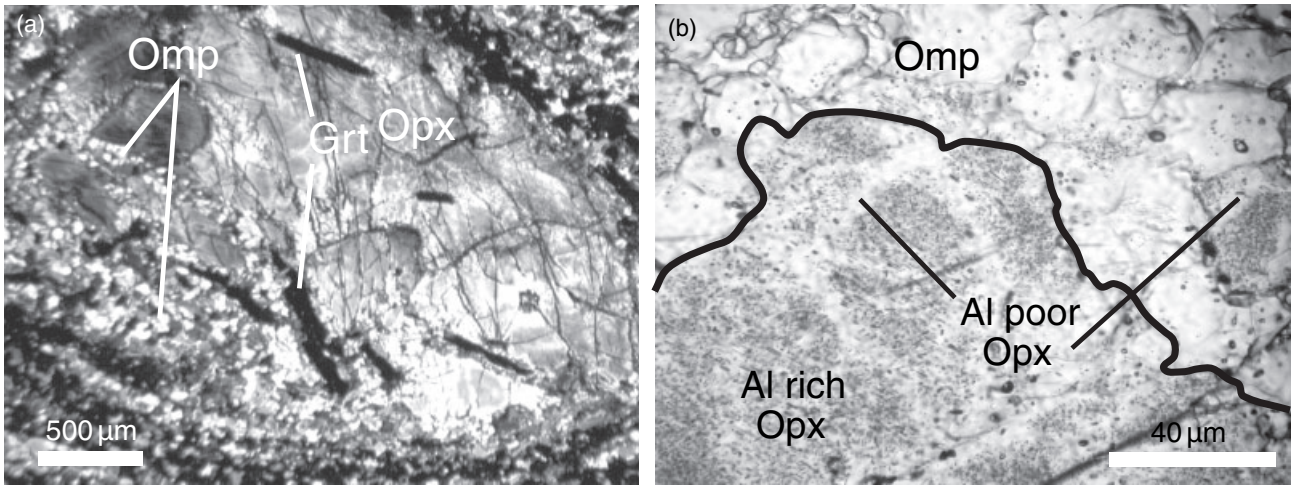

Fig. 3. Photomicrographs of the mylonitic sample showing a prophyroclast of orthopyroxene (a) and a closeup of a view of annealed fractures in orthopyroxene (b).

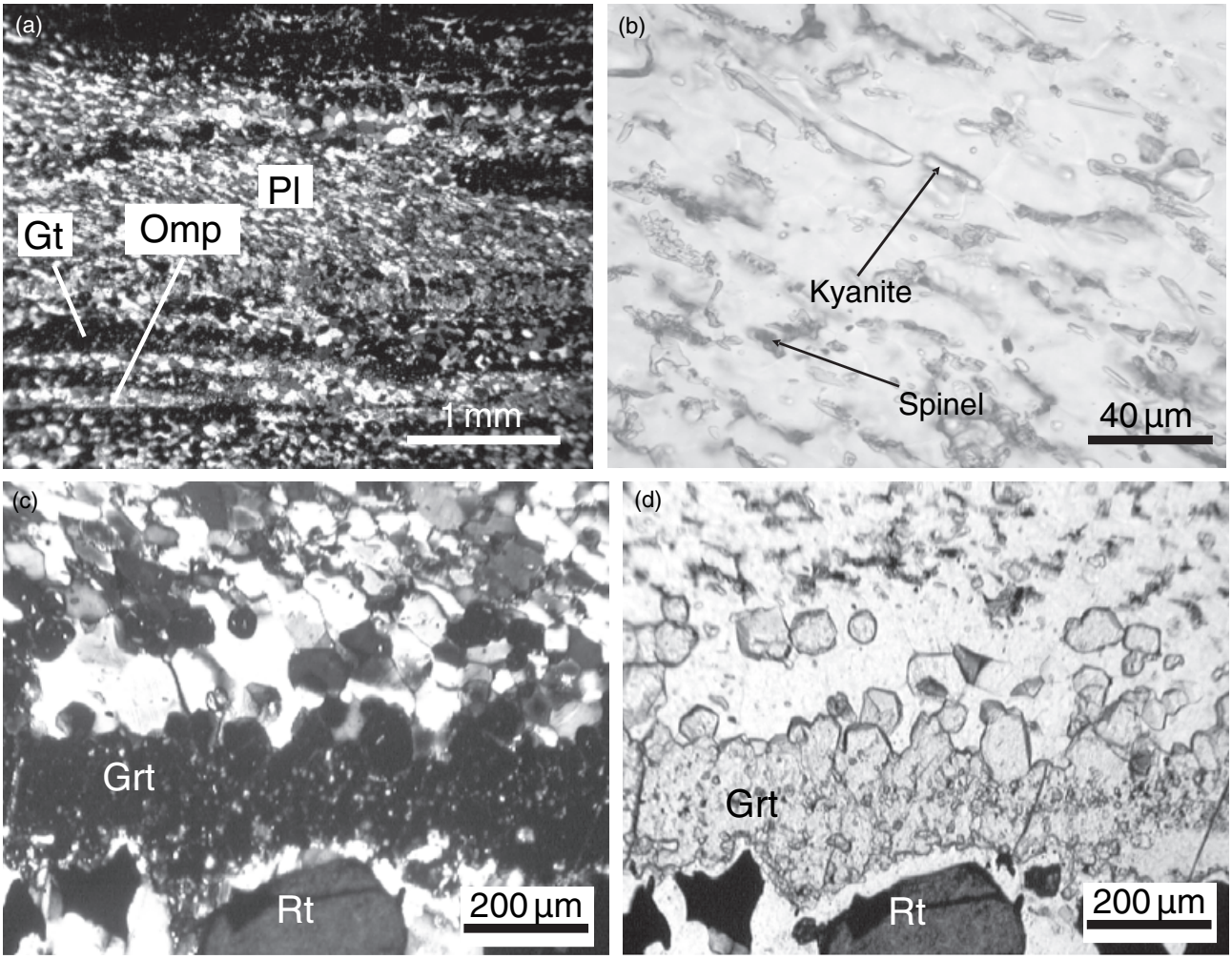

Fig. 4. (a) Photomicrograph in crossed polarized light of oblique foliation in plagioclase-rich layer. (b) Kyanite and spinel in plagioclase-rich layers that has a strong oblique foliation. Photomicrographs of the mylonitic gabbro in plane (c) and crossed polarized light (d) that show loss of grain shape-preferred orientation plagioclase, loss of spinel and euhedral garnet at the outer part of the garnet corona.

retrograde metamorphism (Terry *et al*., 2000). An oblique grain shape orientation at an angle of up to 45° to the foliation can be recognized in the centre of the plagioclase layers (Fig. 4a). In contact with the garnet layers, plagioclase is coarser grained and more Na-rich, kyanite and spinel are lost from the assemblage, and grain shape-preferred orientation (SPO) is not present (Fig. 4c,d).

The CPO of plagioclase in the foliated sample shows large domains with similar orientations. These correspond to the recrystallized lenses that represent the original grains from the igneous structure. However, different lenses show very different CPOs indicating that these are still influenced by the original grain orientations. Similar observations were made by Prior & Wheeler (1999) and Jiang *et al*. (2000) in an albite-rich mylonite. As a result of the large size of the lenses relative to the sample, the combined texture is probably not really representative for the bulk sample. In the mylonitic sample, areas with oblique SPO (Figs 4a & 5a) show a weak CPO where the {0 0 1} poles are aligned at a high angle to the pole of the foliation and the ⟨1 0 0⟩ directions form a girdle perpendicular to this maximum (Fig. 5b). This indicates that intracrystalline glide on the (0 0 1)[1 0 0] slip system was involved during the deformation of plagioclase. In the mylonite, however, no CPO is discernible.

Ilmenite/magnetite layers

Ilmenite and magnetite occur in layers that appear to be pinched out and wrap around original igneous porphyroclasts. Both ilmenite and magnetite form euhedral to subhedral grains with little or no signs of internal deformation or any obvious grain SPO (Figs 6 & 7a). Ilmenite grains display undeformed exsolution lamellae of hematite (Fig. 7a). The layers decrease dramatically in thickness with increasing

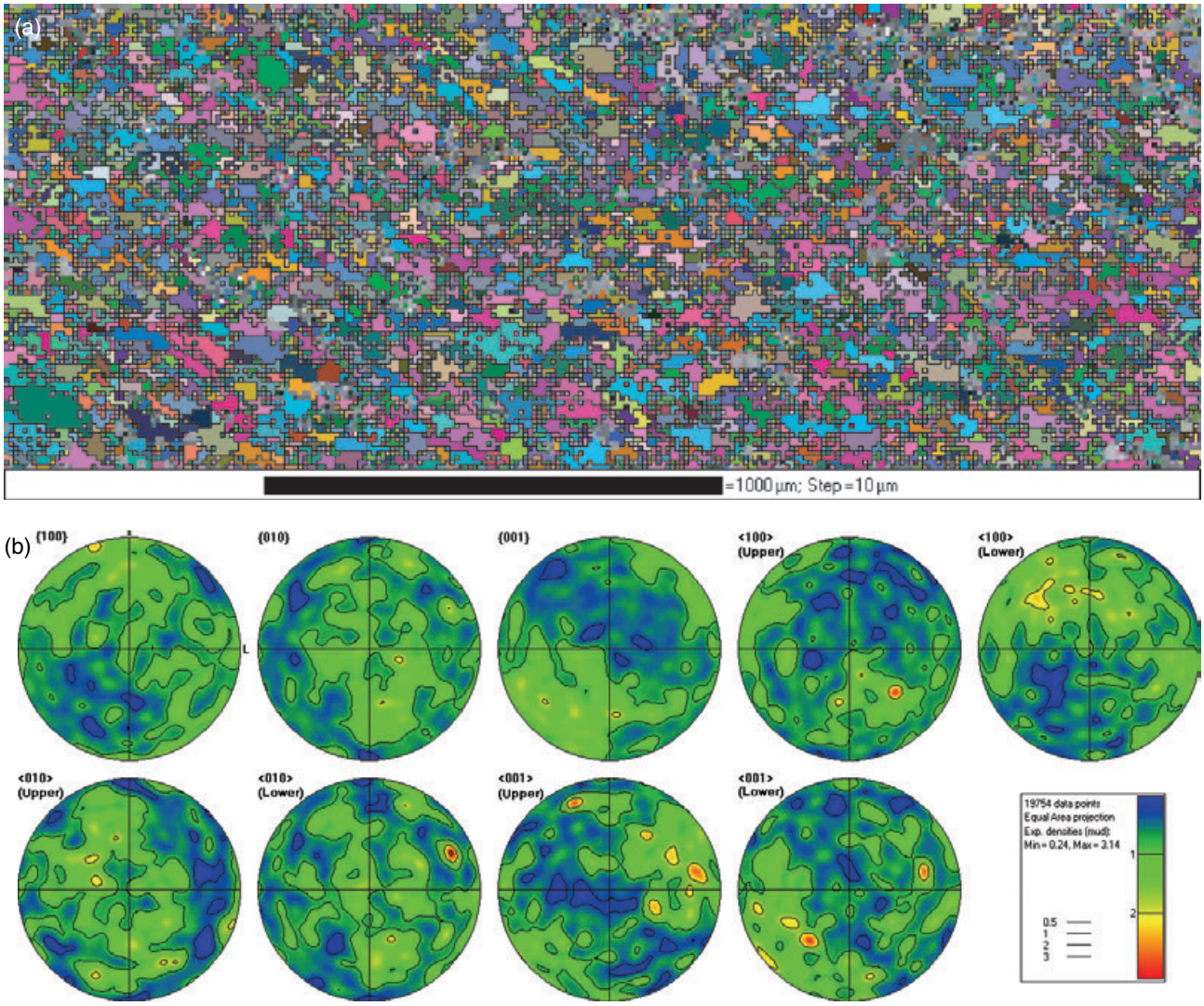

Fig. 5. (a) Microstructural map resulting from an automated EBSD measurement in a plagioclase layer of the mylonitic sample; grains were reconstructed by drawing grain boundaries (black) for misorientations $>10°$; colouring of grains is arbitrary according to orientation; grey points are minerals other than plagioclase; (b) pole figures for the plagioclase layer in (a); pole to foliation is on top (**s**) and the lineation is horizontal (**L**); shear sense from SPO is sinistral, lower hemisphere projection except for $\langle 1\ 0\ 0\rangle$, $\langle 0\ 1\ 0\rangle$ and $\langle 0\ 0\ 1\rangle$, where both hemispheres are shown.

deformation but remain as continuous bands in the microstructure.

Both ilmenite and magnetite show CPOs (Fig. 8): in ilmenite the basal plane $\{0\ 0\ 1\}$ is preferentially aligned subparallel to the foliation and both $\{1\ 0\ 0\}$ and $\{1\ 1\ 0\}$ poles cluster around the lineation. This CPO can be explained by basal glide in the **a** direction which is the most easily activated slip system in the trigonal structure of ilmenite (Bascou *et al.*, 2002). A submaximum of $\{0\ 0\ 1\}$ poles lies in the intermediate fabric direction, i.e. in the foliation and perpendicular to the lineation (Fig. 8). This submaximum becomes stronger in the more deformed samples and is indicative of intracrystalline glide on the prism planes in the **a** direction. The activation of this second slip system is most likely due to the higher strains that have been accommodated in the mylonitic and mylonite samples.

In magnetite, the CPO is not as clear since the number of grains is much lower; however, the $\{1\ 0\ 0\}$ pole figure shows a concentration of poles close to the pole of the foliation, slightly (20–30°) rotated against the sense of shear. The $\{1\ 1\ 0\}$ pole figure also shows a concentration of poles close to the lineation, again rotated 20–30° against the sense of shear. In the spinel structure of magnetite, the oxygen atoms form a face-centred sublattice which favours the $\langle 1\ 1\ 0\rangle$ as Burgers vector (slip direction) and $\{1\ 1\ 1\}$ as well as $\{1\ 1\ 0\}$ as possible glide planes (Mitchell, 1999). The weak CPO of magnetite in this sample may therefore be due to intracrystalline glide.

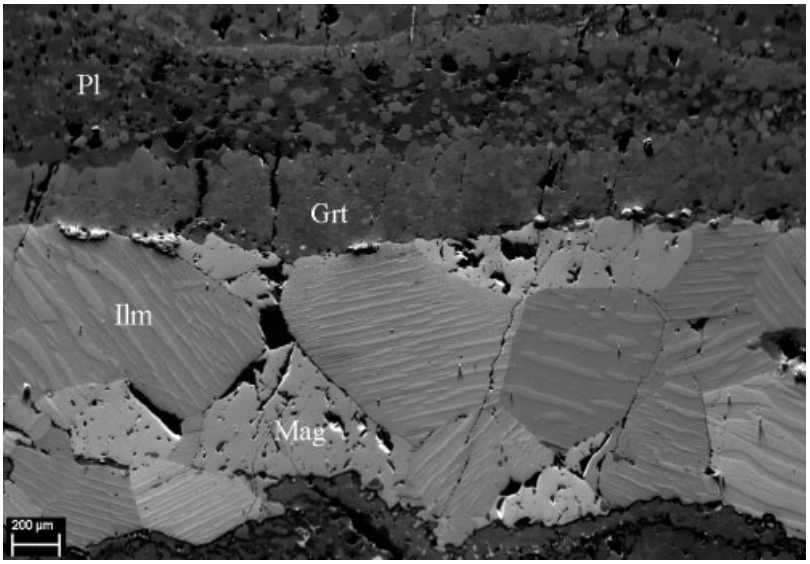

Fig. 6. SEM-BSE image showing the Z contrast in an ilmenite–magnetite layer (bottom) and adjacent layers of garnet and plagioclase (top) in the foliated sample; note change in grain size in the garnet layer from bottom (fine) to top (coarse).

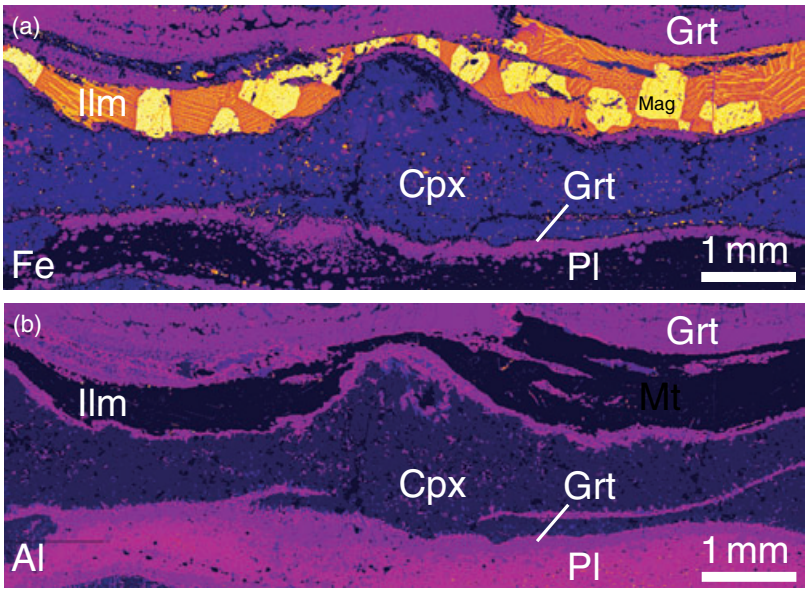

Fig. 7. Element distribution maps of Fe (a) and Al (b) in the foliated sample (1629).

Omphacite layers

Omphacite occurs in layers that are commonly bounded by layers of garnet and in strain shadows around igneous orthopyroxene. The aggregates are fine grained and equigranular with good triple-point grain boundaries (Figs 4a & 9). Omphacite shows no grain SPO observable in the petrographic microscope as is commonly seen in deformed eclogite lenses and shear zones. However, the apparent lack of SPO does not preclude the existence of a CPO. In both the mylonitic and the mylonite sample, results from the SEM-EBSD analysis show an alignment of ⟨0 0 1⟩ axes parallel to the lineation, whereas {1 0 0}, {0 1 0} and {1 1 0} poles form less well-defined broad girdles at high angles to the shear direction (Fig. 10). The **c** direction in omphacite corresponds to the direction of the Burgers vector of some of the most common slip systems in clinopyroxene (1 0 0)[0 0 1] or (1 1 0)[0 0 1] (e.g. Godard & van Roermund, 1995), indicating that slip on these systems was active during deformation. The CPOs are not very strong (maximum densities at 2.5 m.r.d.) because of the concurrent dynamic recrystallization, which tends to weaken crystallographic alignments.

Garnet layers

Garnet in corona structures in weakly deformed to mylonitic samples shows a characteristic change in grain size (Fig. 6). Fine-grained areas commonly show

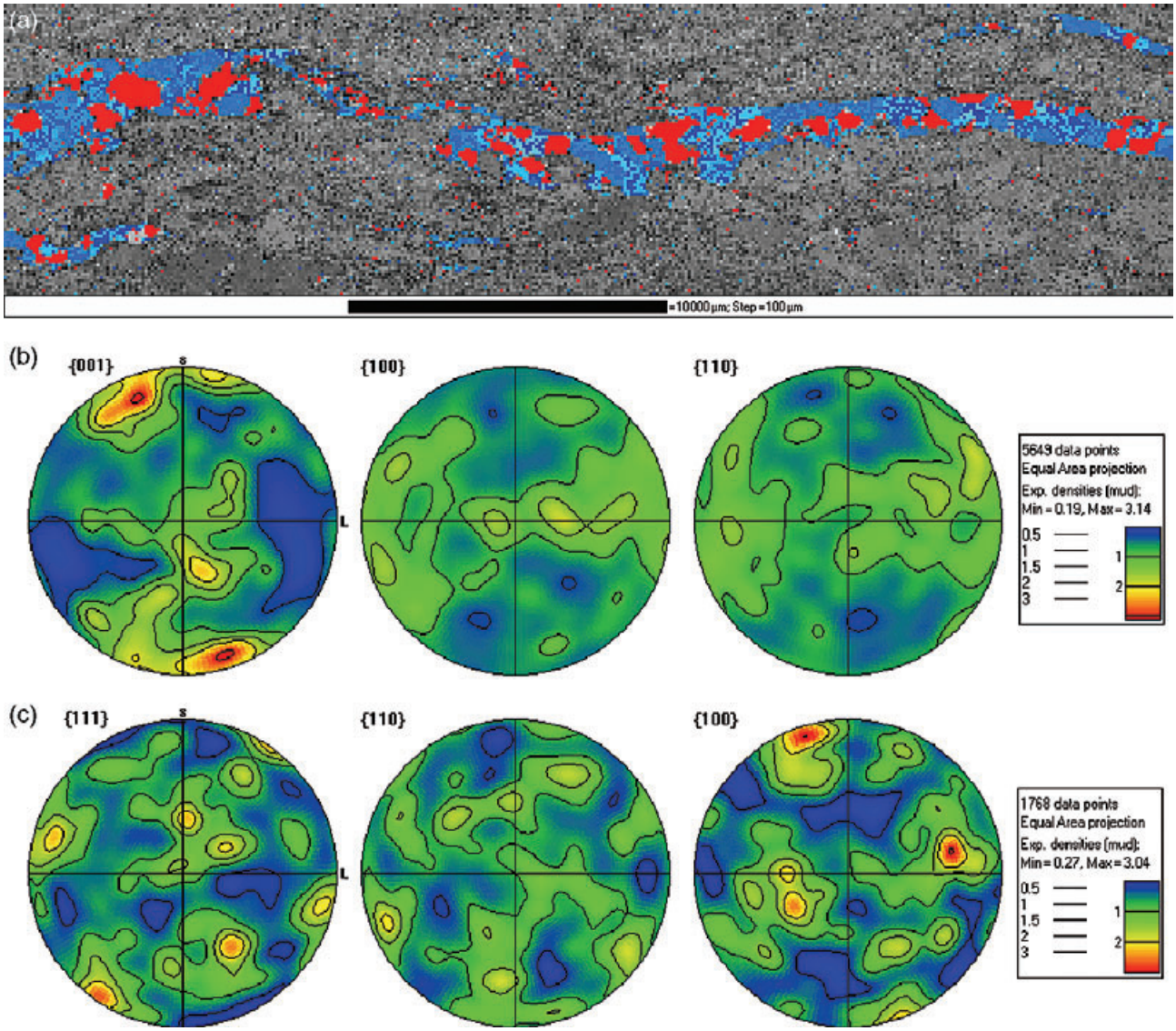

Fig. 8. (a) Microstructural map resulting from an automated EBSD measurement in an ilmenite–magnetite layer of the foliated sample; ilmenite and magnetite are shaded in blue and red, respectively, shading is arbitrary according to orientation; grey points are phases other than ilmenite or magnetite; (b) pole figures of ilmenite in (a); (c) pole figures of magnetite in (a); orientation and projection in (b) and (c) are the same as in Fig. 5; shear sense is dextral.

a grain SPO, whereas the coarse rims typically display euhedral crystals growing into the matrix (Fig. 11). The overall CPO of the garnet is random and also on a local scale, i.e. in the fine grained areas no CPO could be detected. The change in grain size is interpreted to be due to syn- to post-kinematic growth and fine-grained garnet deformed mainly by diffusion-accommodated grain-boundary sliding (Terry & Heidelbach, 2004). The grain size in the fine grained layers decreases with increasing deformation, ranging from *c.* 33 μm in the foliated sample to *c.* 8.5 μm in the mylonitic sample. The microstructures do not indicate a significant strength contrast with the surrounding minerals (ilmenite, omphacite and plagioclase). This behaviour and deformation mechanism is thought to result from the very fine initial grain size (Terry & Heidelbach, 2004).

Composition maps nicely define the break between the syn- and post-kinematic growths of garnet. The break corresponds to a change in the grossular component of garnet (Fig. 11). There is no strong increase in the almandine component in the outer part along the chemical traverse X–X' which is interpreted to be due to the relatively slow diffusion of Ca compared with Fe (Fig. 11). This change in the Ca concentration represents heterogeneity at the scale of the garnet layer. In addition, there is also compositional heterogeneity on the grain scale which is observed in high-resolution composition and BSE maps acquired using high sample currents (Fig. 12).

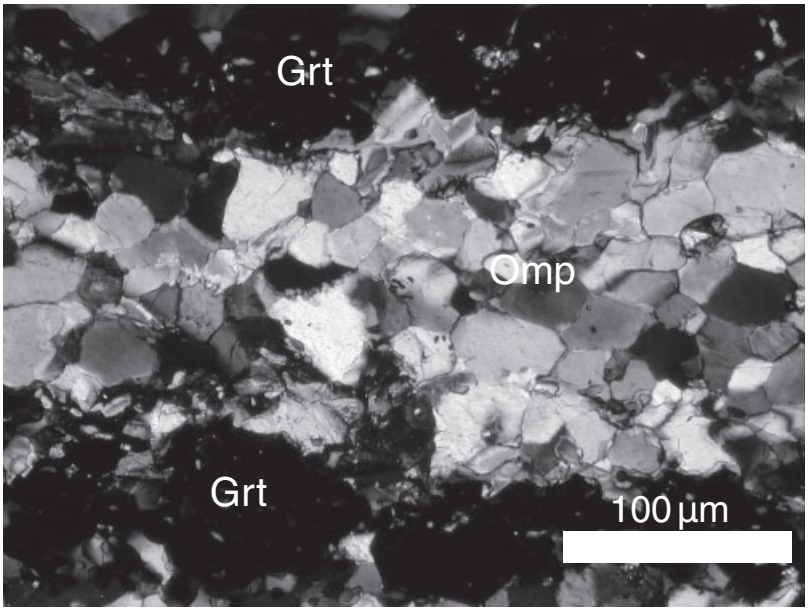

Fig. 9. Photomicrograph in crossed-polarized light of an omphacite layer bounded by garnet layers from the mylonitic sample (453).

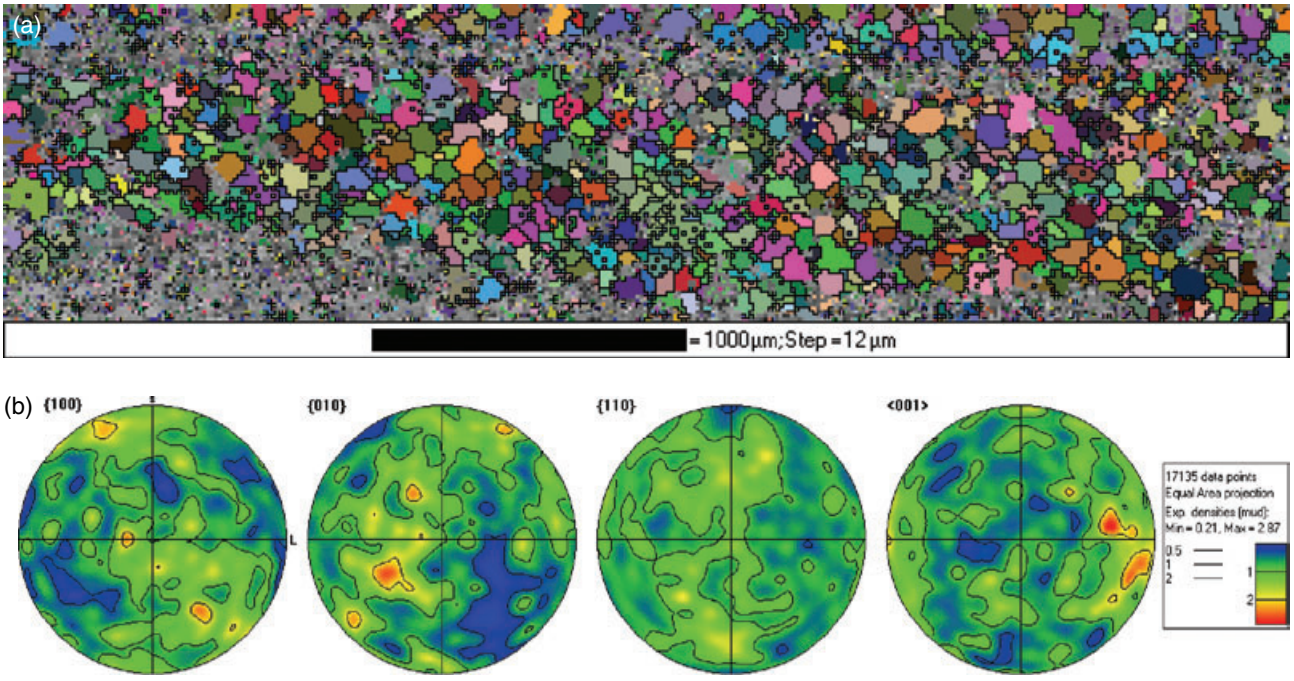

Fig. 10. (a) Microstructural map resulting from an automated EBSD measurement in an omphacite layer of the mylonitic sample; grains were reconstructed by drawing grain boundaries (black) for misorientations $> 10°$; colouring of grains is arbitrary according to orientation; grey points are minerals other than omphacite; (b) pole figures of the omphacite layer in (a); orientation and projection is the same as in Fig. 5; shear sense is sinistral.

These maps show a combination of compositional and orientation contrast effects that result from differences in lattice orientation. The grain boundaries can be identified in most cases by using a combination of both composition maps and the BSE images. The grains of garnet have curved boundaries and appear to show a weak grain SPO. The grains show complex zoning: some grains show an increase in Ca from core to rim in contrast to others that display decreasing Ca from core to rim (grains labelled 1 and 2 in Fig. 12). Additionally, some grains show no systematic zoning as well as truncation of complex zoning against other grains. The preservation of layer- and grain-scale heterogeneities give

insights into processes that enhance metamorphic reactions.

MICROSTRUCTURAL EVOLUTION AND CONDITIONS OF METAMORPHISM

The microstructural and metamorphic evolution observed in these rocks is shown in Fig. 13. The earliest part of the Scandian metamorphism and deformation is preserved in porphyroclasts of Al-rich igneous orthopyroxene (Fig. 3a) where annealed fractures composed of Al-poor pyroxene are truncated by omphacite (Fig. 3b) and in the centre of plagioclase layers where a strong SPO is present (Fig. 4a,c). The consumption of spinel in reactions (2) and (3) (Fig. 4c,d) and preservation of kyanite and spinel in the central part of plagioclase layers indicate that the end-member reaction

$$\text{Al-rich orthopyroxene} = \text{Al-poor orthopyroxene} + \text{kyanite} + \text{spinel} \quad (4)$$

took place on the prograde path (Table 1). Spinel is stable on the low temperature side of reaction (4) which was overstepped during cooling of the gabbro prior to the Scandian metamorphism. It is important to note that the time at which garnet entered the assemblage is not known and depends on the bulk composition but is reasonable to assume that garnet pre-dates reaction (4) as it is a reactant in reactions (2) and (3).

Reaction (4) was used to determine the conditions on the prograde path. Metamorphic conditions were estimated using the technique of Berman (1991) with the TWQ program version 2.02 which is identical approach of Terry *et al.* (2000) in order to maintain internal consistency for comparison of conditions. Reaction (4) is strongly temperature-dependent and a range of orthopyroxene compositions yield conditions of *c.* 500–650 °C. Pressure is constrained between 0.5 and 1.4 GPa by the presence of plagioclase and kyanite and it is likely that these rocks underwent prograde metamorphism at amphibolite facies which is consistent with other HP and UHP rocks in this region that record a prograde history.

Deformation continued along the prograde path and the major minerals involved in the garnet-forming reactions show signs of plastic deformation. The CPOs in omphacite, plagioclase, ilmenite and magnetite indicate that intracrystalline deformation mechanisms were active during the formation of these minerals. The microstructures in the fine-grained garnet layers show that it deformed by diffusion-assisted grain-boundary sliding. The deformation that is reflected in these microstructures and CPOs is clearly related to the formation of the foliation and lineation that characterize the rocks in the shear zones and foliated parts of the Haram gabbro.

The timing of reaction (3) relative to deformation is illustrated by the microstructure in the mylonitic sample. The consumption of spinel was clearly associated with the growth of euhedral garnet and coarse-grained plagioclase that has no grain SPO (Fig. 4c,d). This indicates that deformation was not active or partitioned away during the growth of these phases. Rutile, a product in reaction (3), occurs on the interior of the layered corona structure as porphyroclasts with asymmetric tails of albitic plagioclase. Ilmenite, a reactant in reaction (3), was deformed into layers and partially replaced by rutile. Plagioclase shows a strong grain SPO. These observations point to two important conclusions: (i) rutile could not have grown without producing garnet and that the rutile grain is a delta clast with tails of plagioclase. (ii) Reaction (3) continued to produce garnet after deformation stopped and was localized in other areas.

At peak metamorphic conditions, all phases including garnet (Figs 4, 10, 11 & 13c), plagioclase (Figs 4c,d & 13c), ilmenite (Fig. 6), magnetite and omphacite (Fig. 9) show microstructural features which are typical for static conditions: the coarse rims of the garnet layers with faceted grains, the adjacent coarse plagioclase with no grain SPO, the recrystallized grain structure of omphacite as well as the large ilmenite and magnetite grains without internal deformation. These microstructures evidence a phase in the history of the Haram gabbro where deformation had largely ceased, and the minerals reacted and recrystallized under static conditions.

The discovery of microdiamonds within the Berdane mantle peridotite on Fjørtoft (Fig. 1) (van Roermund *et al.*, 2002) and pressure and temperature estimates of 875 °C and 4.1 GPa, respectively (Carswell & van Roermund, 2005) imply UHP conditions for the surrounding enclosing gneiss which is the host for the Haram gabbro. These estimates are in general agreement with the revised estimates (Terry & Robinson, 2001) of 820 °C and 3.2 GPa using the thermobarometers of Ravna & Terry (2004) from a kyanite eclogite containing the assemblage kyanite + garnet + omphacite + zoisite + prismatic pseudomorphs of polycrystalline quartz after coesite (Terry *et al.*, 2000). The difficulty with assigning these extreme *P–T* conditions has been the absence of UHP indicators in crustal eclogite lenses that cannot be reasonably associated with UHP lithologies, the very close proximity of the proposed HP–UHP contact (Carswell & Cuthbert, 2003; Terry & Robinson, 2004). However, new pressure and temperature estimates of 820 °C and 3.1 GPa, respectively, were obtained for the Kvalvika peridotite which is also enclosed in the Ulla gneiss (Terry *et al.*, 2005). In this case, the eclogitized Ulla gneiss and the Kvalvika peridotite have the same structural fabric indicating that both had experienced UHP conditions. Thus, the results above indicate that deformation in the Haram gabbro ceased some time

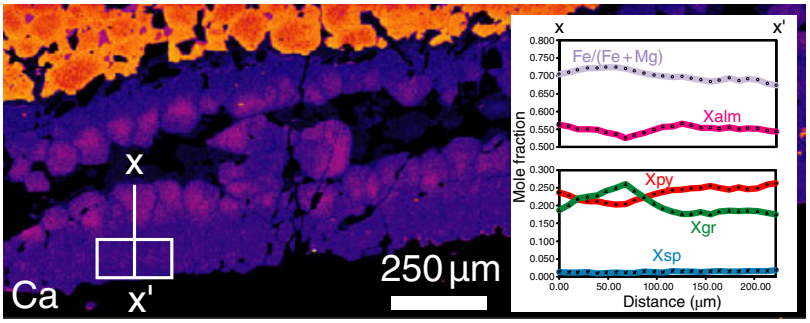

Fig. 11. Element distribution map of Ca in garnet layers in the foliated sample (1629) and compositional changes along *X*–*X*′ (c). Box in (a) shows the location of Fig. 12.

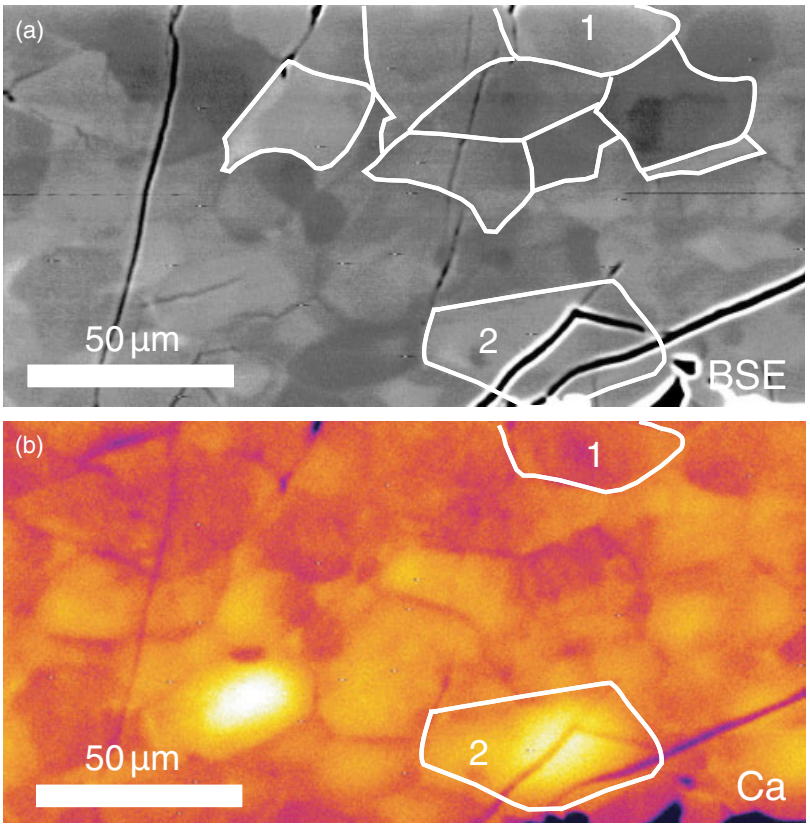

Fig. 12. Backscattered electron image of syntectonic garnet (a) and element distribution map of Ca (b). See Fig. 11 for location. Numbers refer to grains discussed in the text.

between about 650 °C and 1.0 GPa and 820 °C and 3.1 GPa. These results indicate that the pressure and temperature values for metamorphosed gabbros of 750 °C and 1.5–2.0 GPa of Mørk (1985) and 780 °C and 1.8 GPa of Terry *et al.* (2000), respectively, are minimum estimates and static growth appears to have occurred at UHP conditions.

The decompression stage is recorded by the growth of plagioclase, clinopyroxene, orthopyroxene symplectite in the mylonitic sample (Terry & Robinson, 2004). The presence of amphibole in the ultramylonite samples and static overprinting of eclogite facies assemblages are associated with fluid infiltration and pegmatite emplacement at 390 ± 2 Ma (Robinson *et al.*, 2003).

THE ROLE OF DEFORMATION IN ENHANCING METAMORPHIC REACTIONS

The microstructure is related to syn- to post-kinematic growth during the prograde evolution of these rocks in both the foliated and mylonitic samples. First, the plagioclase-rich layers show kyanite and spinel throughout, indicating that the entire layer was involved in reaction (4) (Figs 2a, 4a & 13). In contrast, post-kinematic growth of garnet and plagioclase is restricted to a very narrow region (Figs 3a,b & 13) and indicates the mass transfer distances of material were significantly shortened after the deformation was partitioned away. The shortening of mass transfer distances is also interpreted to be partly responsible for

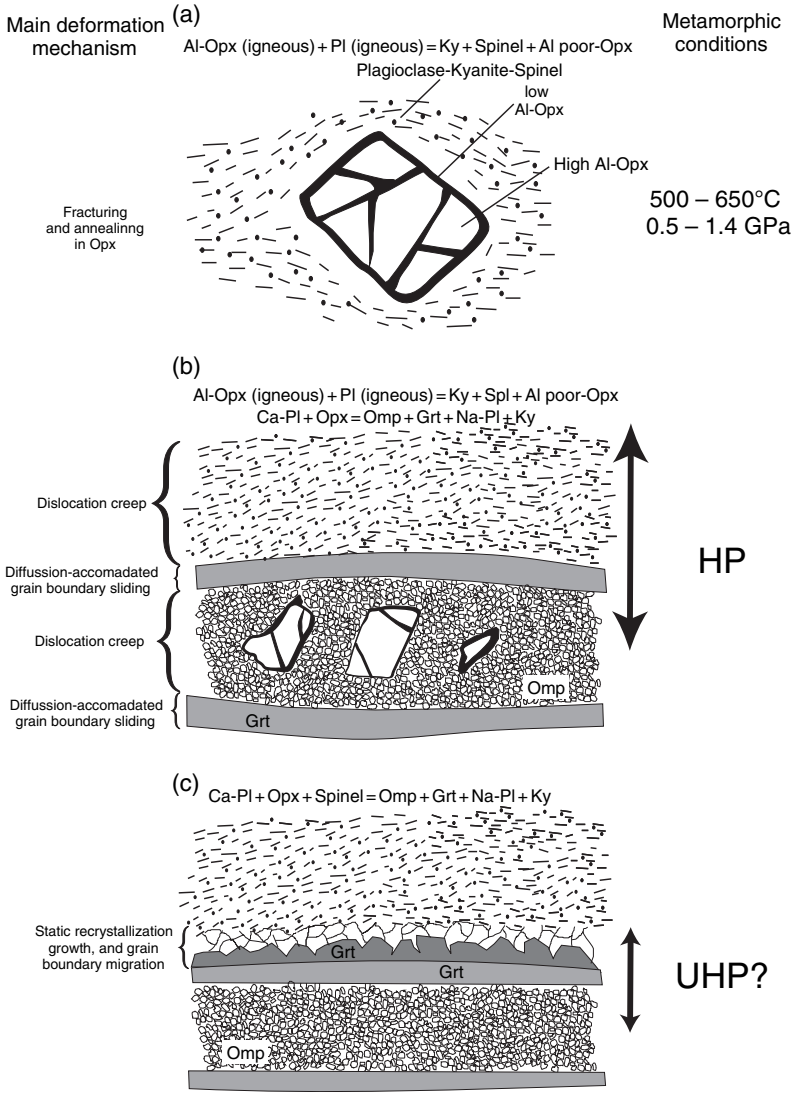

Fig. 13. Evolutionary diagram for syn- to post-kinematic for the eclogite shear zones in the Haram gabbro. The arrows represent the diffusion distances inferred from compositional mapping, microstructure, and mineral chemistry.

layer-scale chemical heterogeneity in both plagioclase (Fig. 7b) and garnet (Fig. 11) as a result of change in the effective bulk composition.

There are a number of ways in which the shortening of the diffusion distances might have occurred in these shear zones (Brodie & Rutter, 1985). The most obvious is cooling but as the sequence of reactions is prograde it is not likely to be the mechanism in this case. The diffusion distances could also have shortened by reducing the permeability of fluids that enhanced the metamorphic reactions. However, the role of fluids is uncertain in these shear zones as there is no evidence for the presence of a free fluid phase during metamorphism although a number of studies conclude that they are required to overcome kinetic barriers associated with eclogite-facies reactions (Früh-Green, 1994; Austrheim *et al*., 1998; Glodny *et al*., 2003; John & Schenk, 2003). No hydrous phases like phengite, zoisite and amphibole or veins related to fluid infiltration are observed in these shear zones. If a fluid was present, diffusion distances may have been increased by enhancing permeability. Diffusion distances may also be shortened by grain size reduction which increases the surface area thereby enhancing reaction progress. The most obvious change that takes place when strain is removed from the shear zone is that the grain size increases where the reaction (3) continues (Fig. 3), indicating that diffusion along grain boundaries played a significant role. The exact mechanism(s) for shortening the diffusion distance is uncertain but it is clear that deformation was the most important influence in these shear zones.

The preservation of grain- and layer-scale heterogeneities seen in garnet gives important information on how deformation may assist in the re-equilibration of rock to a new set of conditions. The deformed part of the garnet layer shows little compositional zoning on the scale of the layer (Fig. 11). However, on the grain

scale, there are complex zoning patterns (Fig. 12) which are interpreted to be the result of two processes. The first is grain-boundary sliding that juxtaposes grains of different composition (mechanical mixing) and thereby homogenizes the composition on the scale of the deformed part of the garnet layer. It is important to note that the lack of an equilibrated grain structure indicated by the complex zoning pattern in Fig. 12 is a feature of deformation and not related to static recrystallization as described by Jessell *et al.* (2003). The second process is migration of grain boundaries that could result in truncation of complex zoning which may be driven by differences in chemical potential on opposite sides of the grain boundary leading to diffusion-induced grain-boundary migration (Poirier, 1985). Alternatively, it can be driven by differences in stored strain (dislocation) energy (e.g. Jessell, 1987). The lack of a CPO makes it unlikely that differences in dislocation densities were the main driving force for grain-boundary migration in the deformed garnet layer which leaves diffusion-induced grain-boundary migration as the main process. Both grain-boundary migration and grain-boundary sliding lead to homogenization of the deformed part of the garnet layer which is seen on the scale of the chemical traverse and chemical maps in Fig. 11. The preservation of complex zoning on the grain scale (Fig. 12) suggests that mixing and grain-boundary diffusion are the dominant mechanisms for chemical homogenization and mass transfer during deformation.

RHEOLOGICAL PROPERTIES OF HP SHEAR ZONES

The rheological properties of polyphase materials are difficult to determine because the mixing behaviour and its effect on the strength of the rock are generally unknown. However, the presence of monomineralic to nearly monomineralic layers of garnet, plagioclase and omphacite in the strained samples and their deformation without necking or breaking indicates that, in a first approximation, the flow laws for these minerals can be applied separately. The similar strengths of these layers suggest that the flow laws for the different minerals might converge at a common differential stress and strain rate. In the following we will therefore apply experimentally determined flow laws for garnet, plagioclase and clinopyroxene to constrain the stresses and strain rates at which the deformation of the Haram gabbro took place.

In Fig. 14 and Table 2, the available rheological data applicable to our case are displayed for the relevant stress–strain rate region. A temperature of 700 °C was assumed and grain sizes of 8.5 and 33 μm for garnet, and 50 μm for plagioclase and omphacite were used in the calculations. For stresses between 100 and 150 MPa, the flow laws of fine-grained garnet (Wang & Ji, 2000) give strain rates between 10^{-13} and 10^{-12} s^{-1} for deformation by diffusional creep.

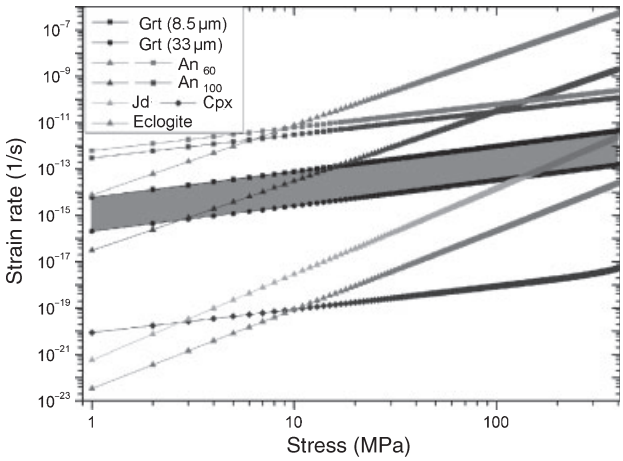

Fig. 14. Stress–strain rate plot showing experimental flow laws for garnet (grt 8.5 μm and grt 33 μm; Wang & Ji, 2000), plagioclase with 60% and 100% anorthite content (an60 and an100; Rybacki & Dresen, 2004), clinopyroxene (cpx; Bystricky & Mackwell, 2001), jadeite (jad; Orzol *et al.*, 2002) and eclogite (Jin *et al.*, 2001). All calculations were carried for a temperature of 700 °C. Symbols indicate diffusion creep (squares, circles), dislocation creep (triangles) and combined dislocation–diffusion creep (diamonds); see Table 2 for experimental details.

Increasing the grain size of garnet from 8.5 to 33 μm reduces the strain rate by about 1.5 orders of magnitude (at constant stress), which may reflect realistically the different deformation rates in different parts of the shear zone. The strength of plagioclase varies with composition and water content; here we only show the difference for pure anorthite and a plagioclase with 60% anorthite content, both of them 'wet', i.e. with 0.07 and 0.3 wt% dissolved water (Rybacki & Dresen, 2004). Except for anorthite deforming by dislocation creep at very low stress (< 10 MPa), plagioclase is generally weaker than fine-grained garnet. Flow laws for 'dry' anorthite (0.004 wt% H_2O content, not shown here) exhibit a dramatic increase in strength bringing its rheology closer to that of clinopyroxene (Rybacki & Dresen, 2004). The flow law of clinopyroxene (diopside) incorporates combined dislocation and diffusion creep and shows an extremely high strength (Bystricky & Mackwell, 2001). For pure jadeite, the strength decreases significantly (Orzol *et al.*, 2002) and reaches similar strain rates (*c.* 5×10^{-13} sec^{-1}) as the coarse grained garnet at a stress of *c.* 150 MPa. The flow law for eclogite (Jin *et al.*, 2001) again shows higher strengths, which is most likely due to the additional coarse garnet. An omphacitite which was also deformed in the study of Jin *et al.* (2001) was significantly weaker than eclogite indicating that the rheology of pure omphacite is more similar to jadeite.

The intersection of jadeite and garnet flow laws makes stresses of 100–150 MPa and strain rates of 10^{-12} to 10^{-13} s^{-1} the most likely deformation conditions for the shear zones in the Haram gabbro. The relatively high stresses are mainly needed for the

Table 2. Rheological parameters for a power law equation of the form: $\epsilon = A\sigma^n d^{-m}\exp(-Q/RT)$ from the literature.

Material	Activation energy (Q) (kJ mol^{-1})	Log preexp. const. (log A) (MPa^{-n} μm^m s^{-1})	Stress exp. (n)	Grain size exp. (m)	Grain size (exper.) (μm)	Grain size (calc.) (μm)	Strain rate (exper.) (s^{-1})	Temperature (exper.) (°C)	Reference
Garnet	347	−5.27	1.1	2.5	4.5	8.5, 33	10^{-7}–10^{-5}	1100–1300	Wang & Ji (2000)
Plagioclase	153(df),235(dl)	1.1(df),−1.5(dl)	1(df),3(dl)	3(df),0(dl)	3.4	50	10^{-6}–10^{-4}	864–1104	Rybacki & Dresen (2004)
(An60, An100)	170(df), 356(dl)	1.7(df),2.6(dl)	1(df),3(dl)	3(df),0(dl)					
Jadeite	326	−3.3	3.7	0	12	–	10^{-6}–10^{-5}(?)	900–1000(?)	Orzol *et al.* (2002)
Diopside	560(df),760(dl)	15.1(df),10.8(dl)	1(df),4.7(dl)	3(df),0(dl)	8	50	10^{-6}–10^{-4}	1100–1250	Bystricky & Mackwell (2001)
Eclogite	480	3.3	3.4	0	30–50	–	$10^{-4.4}$–$10^{-3.2}$	1177–1327	Jin *et al.* (2001)

The parameters were used for the calculation of stress–strain rate curves in Fig. 14; for diopside a flow law combining diffusion and dislocation creep law was used.
df, diffusion creep law; dl, dislocation creep.

deformation of jadeite/omphacite; the mechanical data for pyroxene are still very scarce, and none exist for diffusional creep, which becomes more important at lower stresses. The influence of pressure on the flow laws was neglected here as there are no systematic studies; the flow laws presented were measured at confining pressures between 300 MPa (plagioclase, clinopyroxene) and 3 GPa (eclogite), indicating that for the pressure range in question (< 3.1 GPa) large effects are unlikely. Another unknown is the water content of the minerals at the time of deformation; from the absence of water-bearing phases it is clear that there was no free water, but the amount of water dissolved in the minerals is not constrained. With the exception of plagioclase, the flow laws were derived at 'dry' conditions, which mean that they give upper bounds in strength and lower bounds on strain rate. Additional water is most likely to decrease the stresses and to increase the strain rates. Keeping also in mind that all of the flow laws above had to be extrapolated considerably to match natural conditions (especially in strain rate, temperature and, to a lesser extent, in grain size and composition) the resulting stress–strain rate conditions of the Haram gabbro seem at least realistic for the prograde deformation of a subducting slab.

IMPLICATIONS

The results of this study have important microstructural, metamorphic and tectonic implications. Microstructural and metamorphic implications include: (i) static post-kinematic recrystallization and growth of a metamorphic mineral can mask CPO and an earlier syntectonic microstructure, which makes the measurement of CPOs with SEM-EBSD an important part of developing *P–T–t–d* histories for metamorphic rocks. (ii) The partitioning of deformation away from the shear zones significantly shortened diffusion distances of elements involved in garnet-forming reactions which implies that deformation considerably enhances metamorphic reactions. (iii) Changes in chemical composition in zoned minerals such as garnet may be caused by deformation. (iv) Changes in chemical composition in metamorphic rocks undergoing deformation are destroyed by a combination of mechanical mixing and grain-boundary migration.

The tectonic implications are related to the changes rheological properties that occur in response to metamorphism in shear zones at HP conditions and include: (i) garnet deformed by diffusion-accommodated grain-boundary sliding and causes a significant weakening (together with plagioclase) relative to a classical eclogite; (ii) the garnet layers appear to have similar strengths as minerals like plagioclase and omphacite that also occur in near monomineralic layers and are deforming at least in part by dislocation creep mechanisms; (iii) the application of experimental flow laws of fine grained garnet, clinopyroxene and plagioclase indicates stresses of 100–150 MPa and strain rates of 10^{-12} to 10^{-13} s^{-1} at 700 °C (HP to UHP) for the deformation of the Haram gabbro. Exhumation rates of millimetre per year to centimetre per year could be therefore accommodated by these shear zones that are tens to hundreds of metres in width at the relatively low differential stresses proposed for the deep part of subduction zones where HP and UHP metamorphism takes place.

ACKNOWLEDGEMENTS

We acknowledge Bayerisches Geoinstitut for providing travel funds and analytical facilities and the Norwegian Geological Survey for providing field equipment for the study. We thank H. Schulze and O. Leitner for sample preparation and D. Krausse for assistance with the electron microprobe. T. Anderson and an anonymous reviewer provided helpful reviews that significantly improved this manuscript.

REFERENCES

Adams, B. L., Wright, S. I. & Kunze, K., 1993. Orientation imaging: the emergence of a new microscopy. *Metallurgical Transactions*, **24A,** 819–833.

Austrheim, H., Erambert, M. & Engvik, A., 1998. Processing of crust in the root of the Caledonian continental collision zone: the role of eclogitization. *Tectonophysics*, **273,** 129–153.

Bascou, J., Raposo, M. I. B., Vauchez, A. & Egydio-Silva, M., 2002. Titanohematite latice-preferred orientation and magnetic anisotropy in high-temperature mylonites. *Earth and Planetary Science Letters*, **198,** 77–92.

Berman, R., 1991. Thermobarometry using multi-equilibrium calculations: a new technique with petrological applications. *Canadian Mineralogist*, **29,** 833–855.

Boundy, T. M., Fountain, D. M. & Austrheim, H., 1992. Structural development and petrofabrics of eclogite facies shear zones, Bergen Arcs, western Norway: implications for deep crustal processes. *Journal of Metamorphic Geology*, **10,** 127–146.

Brodie, K. H. & Rutter, E. H., 1985. On the relationships between defomation and metamorphism with special reference to the behavior of basic rocks. In: *Metamorphic Reactions: Kinetics, Textures and Defomation* (eds Thompson, A. B. & Rubie, D. C.), pp. 138–179. Springer, Berlin.

Bystricky, M. & Mackwell, S. J., 2001. Creep of dry clinopyroxene aggregates. *Journal of Geophysical Research*, **106B,** 13443–13454.

Carswell, D. A. & Cuthbert, S. J., 2003. Ultrahigh pressure metamorphism in the Western Gneiss Region of Norway. In: *Ultrahigh Pressure Metamorphism*. (eds Carswell, D. A. & Compagnoni, R.), *EMU Notes in Mineralogy*, **5,** 51–73.

Carswell, D. A. & van Roermund, H. L. M., 2005. On multi-phase mineral inclusions associated with microdiamond formation in mantle-derived peridotite lens at Bardane on Fjørtoft, west Norway. *European Journal of Mineralogy*, **17,** 31–42.

Cox, R. A. & Indares, A., 1999. Transformation of Fe-Ti gabbro to coronite, eclogite and amphibolite in the Bair du Nord segment, Manicouagan imbricate zone, Eastern Grenville Province. *Journal of Metamorphic Geology*, **17,** 537–555.

Früh-Green, G., 1994. Interdependence of deformation, fluid infiltration and reaction progress recorded in eclogitic metagraitoids (Sesia Zone, Western Alps). *Journal of Metamorphic Geology*, **12,** 327–343.

Glodny, J., Austrheim, H., Molina, J. F., Rusin, A. & Seward, D., 2003. Rb/Sr record of fluid-rock interaction in eclogites: The Marun-Keu complex, Polar Urals, Russia. *Geochemica et Cosmochimica Acta*, **67,** 4353–4371.

Godard, G. & van Roermund, H. L. M., 1995. Deformation-induced clinopyroxene fabrics from eclogites. *Journal of Structural Geology*, **17,** 1425–1443.

Jessell, M. W., 1987. Grain-boundary migration microstructures in naturally deformed quartzite. *Journal of Structural Geology*, **9,** 1007–1014.

Jessell, M. J., Kostrenko, O. & Jamtveit, B., 2003. The preservation of potential microstructures during static grain growth. *Journal of Metamorphic Geology*, **21,** 481–491.

Jiang, Z., Prior, D. J. & Wheeler, J., 2000. Albite crystallographic preferred orientation and grain misorientation distribution in a low-grade mylonite: implications for granular flow. *Journal of Structural Geology*, **22,** 1663–1674.

Jin, Z.-M., Zhang, J., Green, H. W. & Jin, S., 2001. Eclogite rheology: Implications for subducted lithosphere. *Geology*, **29,** 667–670.

John, T. & Schenk, V., 2003. Partial eclogitisation of gabbroic rocks in a late Precambrian subduction zone (Zambia): prograde metamorphism triggered by fluid infiltration. *Contributions to Mineralogy and Petrology*, **146,** 174–191.

Koons, P. O., Rubie, D. C. & Früh-Green, G., 1987. The effects of disequilibrium and deformation on the mineralogical evolution of quartz diorite during metamorphism in the eclogite facies. *Journal of Petrology*, **28,** 679–700.

Mitchell, T. E., 1999. Dislocations and Mechanical Properties of MgO-Al_2O_3 Spinel Single Crystals. *Journal of the American Ceramics Society*, **82,** 3305–3316.

Mørk, M. B. E., 1985. A gabbro to eclogite transition on Flemsøy, Sunnmøre, western Norway. *Chemical Geology*, **50,** 283–310.

Orzol, J., Stöckhert, B. & Rummel, F., 2002. An Experimental Study of the Rheology of Jadeite. *Eos Transactions AGU*, **83,** F602.

Poirier, J. P., 1985. *Creep of Crystals: High-temperature Deformation Processes in Metals, Ceramics and Minerals*. Cambridge University Press, Cambridge.

Pouchou, J. L. & Pichoir, F., 1984a, A new model for quantitative X-ray microanalysis, Part I: application to homogeneous samples. *La Recherche Aerospatiale*, **3,** 13–38.

Pouchou, J. L. & Pichoir, F., 1984b, A new model for quantitative X-ray microanalysis, Part II: application to in-depth analysis of heterogeneous samples. *La Recherche Aerospatiale*, **5,** 47–65.

Prior, D. J. & Wheeler, J., 1999. Feldspar fabrics in a greenschist facies albite-rich mylonite from electron backscatter diffraction. *Tectonophysics*, **303,** 29–49.

Prior, D. J., Trimby, P. W., Weber, U. D. & Dingley, D. J., 1996. Orientation contrast imaging of microstructures in rocks using forescatter detectors in the scanning electron microscope. *Mineralogical Magazine*, **60,** 859–869.

Ravna, E. J. K. & Terry, M., 2004. Geothermobarometry of UHP and HP eclogites and schists – an evaluation of equilibria among garnet-clinopyroxene-kyanite-phengite-coesite/quartz. *Journal of Metamorphic Geology*, **22,** 579–592.

Robinson, P., Terry, M. P., Carswell, D. A., *et al*. 2003. *Tectonostratigraphic Setting, Structure, and Petrology of HP and UHP Metamorphic Rocks and Garnet Peridotites in the Western Gneiss Region, More and Romsdal, Norway*. Norges geologiske undersokelse, Trondheim, pp. 142.

van Roermund, H. L. M., Carswell, D. A., Drury, M. R. & Heijboer, T. C., 2002. Microdiamonds in a megacrystic garnet websterite pod from Bardane on the island of Fjørtoft, western Norway: evidence for diamond formation in mantle rocks during deep continental subduction. *Geology*, **30,** 959–962.

Rubie, D. C., 1983. Reaction-enhanced ductility: the role of solid-solid univarient reactions in deformation of the crust and mantle. *Tectonophysics*, **96,** 331–352.

Rybacki, E. & Dresen, G., 2004. Deformation mechanism maps for feldspar rocks. *Tectonophysics*, **382,** 173–187.

Terry, M. P. & Heidelbach, F., 2004. Superplasticity in garnet from eclogite facies shear zones in the Haram Gabbro, Haramsøya, Norway. *Geology*, **32,** 281–284.

Terry, M. P. & Robinson, P., 2001, *Evidence for Supersilicic Pyroxene in an UHP Kyanite Eclogite, Western Gneiss Region, Norway*. Lunar and Planetary Institute, Houston. Lunar and Planetary Institute Contributions No, 1088, 3842.

Terry, M. P. & Robinson, P., 2003. Evolution of amphibolite-facies structural features and boundary conditions for deformation during exhumation of high- and ultrahigh-pressure rocks, Nordøyane, Western Gneiss Region, Norway. *Tectonics*, **22,** 10-1–10-23, doi: 10.1029/2001TC001349.

Terry, M. P. & Robinson, P., 2004. Geometry of eclogite-facies strcutural features: Implications for production and exhumation of ultrahigh-pressure and high-pressure rocks, Western Gneiss Region, Norway. *Tectonics*, **23,** doi: 10.1029/2002TC001401.

Terry, M. P., Robinson, P. & Ravna, E. J. K., 2000. Kyanite eclogite thermobarometry and evidence for thrusting of UHP over HP metamorphic rocks, Nordoyane, Western Gneiss region, Norway. *American Mineralogist*, **85,** 1637–1650.

Terry, M. P., Heidelbach, F., Couvy, H., Bromiley, G. D. & Ravna, E. J. K., 2005. PT history from the Kvalvika mantle peridotite, Norway: Implications for crust-mantle interactions and conditions and timing for olivine c-slip during continental subduction. *Geological Society of America Absracts with Programs*, **37,** No. 95480.

Wang, Z. C. & Ji, S., 2000. Diffusion creep of fine-grained garnetite: implications for the flow strength of subducting slabs. *Geophysical Research Letters*, **27,** 2333–2336.

Williams, M. L., Melis, E. A., Kopf, C. F. & Hamner, S., 2000, Microstructural tectonometamorphic processes and the development of gneissic layering: a mechanism for metamorphic segregation. *Journal of Metamorphic Geology*, **18,** 41–57.

Received 1 September 2004; revision accepted 1 September 2004.